Journal of Materials Chemistry A

Charge Separation Boosts Exciton Diffusion in Fused Ring Electron Acceptors

Journal:	*Journal of Materials Chemistry A*
Manuscript ID	TA-ART-09-2020-008666.R1
Article Type:	Paper
Date Submitted by the Author:	15-Oct-2020
Complete List of Authors:	Liu, Junyi; California State University Northridge Li, Zi; Institute of Applied Physics and Computational Mathematics Wang, Jiayu; Peking University, College of Engineering Zhang, Xu; California State University Northridge, Physics and Astronomy Zhan, Xiaowei; Peking University, Department of Materials Science and Engineering, College of Engineering Lu, Gang; California State University Northridge, Physics and Astronomy

Charge Separation Boosts Exciton Diffusion in Fused Ring Electron Acceptors

Junyi Liu[†], Zi Li[‡], Jiayu Wang[§], Xu Zhang[†], Xiaowei Zhan[§] and Gang Lu[*,†]

[†]Department of Physics and Astronomy, California State University Northridge, California 91330-8268, United States

[‡]Institute of Applied Physics and Computational Mathematics, P.O. Box 8009, Beijing 100088, China

[§]Department of Materials Science and Engineering, College of Engineering, Key Laboratory of Polymer Chemistry and Physics of Ministry of Education, Peking University, Beijing 100871, China

Abstract

Non-fullerene acceptors (NFAs) are highly promising materials for organic photovoltaics (OPVs). Exciton diffusion in NFAs is crucial to their photovoltaic performance, but is not yet well understood. Here we systematically examine exciton diffusion in a fused-ring electron acceptor (IDIC) based on a first-principles framework. We discover that low-energy excitons in disordered IDIC are charge-separated with electron and hole residing at neighboring molecules, yielding long exciton lifetimes. With low energetic disorder, high exciton density of states (DOS) and long lifetimes, the disordered IDIC is predicted to exhibit large exciton diffusion lengths and high quantum efficiency. The temperature and energy dependences of exciton diffusion are explored and how various materials properties (exciton energy, DOS, energetic disorder, and phonon frequency) conspire to influence exciton diffusion is elucidated. Finally, we show that dilation could be an effective strategy to increase exciton diffusion length in IDIC.

Introduction

In recent years, non-fullerene-acceptors have emerged as highly promising materials in solution-processed organic photovoltaics[1-4], thanks to rapid increase of their power conversion efficiencies (PCEs), now exceeding 18% for single-junction cells[5] and 17% for tandem cells[6]. In contrast to fullerene-based acceptors, NFAs offer greater tunability of bandgaps and energy levels, higher thermal, photochemical and morphological stability[1-4]. On the one hand, NFAs exhibit strong absorption in the visible and near-infrared range[2, 7-10], enabling higher short-circuit current densities. On the other hand, energy losses are lowered in NFAs as compared to fullerene-based acceptors[11-13], enabling higher open-circuit voltage.

Exciton diffusion is a crucial process for photocurrent generation as photo-generated excitons must reach the donor/acceptor interfaces within their lifetimes for charge separation[14]. Hence, exciton diffusion length (L_D) is a key material parameter determining quantum efficiencies of OPVs. However, compared to other material parameters, such as optical absorption[2, 15], carrier mobility[16-18], molecular packing and morphology[19-21], much less attention has been paid to L_D. Even in the research of exciton diffusion[22-25], the focus has been placed on donor materials. Although many NFAs have been developed,[1-4] the study of exciton diffusion in NFAs has remained scarce.[26] Indeed, very little is known about exciton diffusion in NFAs, which hinders future development of NFA-based OPVs. It is to fill this crucial knowledge gap that motivates the present work.

Theoretically, exciton diffusion in organic materials has been studied by using Forster-type energy transfer models, where exciton transition rates are determined either by an empirical Miller-Abrahams form[27, 28] or quantum chemical calculations[29-31]. These approaches are often based on perturbation theories and assume Gaussian distributions for exciton density of states

and/or harmonic approximations for molecular vibrations, whose validity is not generally established. In addition, these approaches are formulated with molecular crystals in mind, and not applicable to amorphous materials. Thus, it is preferable to study exciton diffusion in organic materials from first-principles. Experimentally, a number of techniques have been developed to measure L_D of singlet excitons in organic materials, including fluorescence quenching in bilayers[32], fluorescence volume quenching[33], exciton-exciton annihilation[34], microwave conductivity[35] and electro-optical measurements[36], etc. The advantages and pitfalls of each technique have been discussed in a recent review covering a large number of organic semiconductors[23]. However, despite impressive experimental advances, it is highly challenging to correlate exciton diffusion with molecular structures of organic materials[22]. In particular, how would physical quantities, such as exciton energy, bandgap, density of states, phonon frequencies, energetic disorder, etc., affect exciton diffusion is yet to be established. How exciton diffusion in donor materials, such as conjugated polymers and small molecules differs from that in NFAs needs to be elucidated. In addition, NFAs with alternating acceptor-donor-acceptor (A-D-A) structure were found to exhibit large exciton diffusion lengths, which is unexpected given their low optical bandgaps. More importantly, there is lack of knowledge in excitonic properties of the A-D-A NFAs, and in particular how the A-D-A structure may promote exciton diffusion remains unclear. To address these open questions, we have to gain a deeper understanding of exciton diffusion in NFAs, preferably from a first-principles perspective.

In this work, we perform first-principles simulations to examine exciton diffusion in a fused-ring electron acceptor, indacenodithiophene (IDT) endcapped with 1,1-dicyanomethylene-3-indanone (IDIC, Figure 1a)[8]. IDIC is a widely used NFA in OPVs with the planar A-D-A molecular structure, and has been intensively studied in past few years[15, 37-40]. Facilely

synthesized, IDIC films show strong absorption in 500-800 nm and exhibit high electron mobility (1.1×10^{-3} cm^2 V^{-1} s^{-1})[8]. Without additional treatments, as-cast OPVs based on the IDIC films have PCEs up to 11.9%[39]. The PCE can further reach 12-13% when IDIC is blended with mid-band gap donor polymers, such as benzodithiophene and difluorobenzotriazole units (FTAZ)[40, 41]. Indeed, IDIC represents an ideal material to study exciton diffusion in NFAs with the A-D-A structure, to reveal the dependence of exciton diffusion on relevant physical quantities, and to explore strategies to boost exciton diffusion in NFAs. Most importantly, we uncover that low-energy excitons in IDIC are charge-separated with electrons and holes residing at neighboring molecules. These charge-separated intermolecular excitons are predicted to boost exciton lifetimes, diffusion lengths and possibly interfacial charge separation in IDIC-based OPVs. We speculate that the charge-separated excitons could also exist in other A-D-A type NFAs and are responsible for their superior photovoltaic performance.

Computational methods

We have developed a first-principles framework in which exciton diffusion is modeled as random walks of excitons in the real and energy spaces. In particular, exciton diffusion in a disordered solid is realized via phonon-assisted transitions between localized excitonic states. Our first-principles framework consists of three components: (1) The determination of energy and many-body wavefunction of each excitonic state. (2) The determination of phonon-assisted transition rates between these excitonic states at a given temperature. (3) Kinetic Monte Carlo (MC) simulations to estimate exciton diffusion length, lifetime and diffusivity based on the phonon-assisted transition rates. The details of the framework can be found elsewhere.[18, 42-45.]

We first perform *ab initio* Born-Oppenheimer molecular dynamics (BOMD) simulations to compute single-particle Kohn-Sham (KS) energy levels and orbitals at each time step, from

which the exciton energies and many-body wavefunctions are determined based on the linear-response time-dependent density functional theory (LR-TDDFT)[46, 47] with optimally tuned, screened and range-separated hybrid exchange-correlation functional (OT-SRSH).[48-50] Based on the generalized Kohn-Sham theory, the OT-SRSH functional captures the correct asymptotic behavior using screened exact exchange for large distances. The TDDFT-OTSRSH method has been used successfully to determine optical bandgap and exciton binding energy in various organic and inorganic semiconductors.[48, 49, 51-54] The time-dependent excitonic wavefunctions are expanded in terms of these many-body wavefunctions, with the expansion coefficients computed from the non-adiabatic molecular dynamics (NAMD) simulations[42, 55]. The diffusing exciton is assumed to occupy an initial many-body state, and each coefficient represents the probability amplitude for the excitonic hopping transition from this initial state to another many-body state. The phonon-assisted excitonic transition rates are determined based on the nonadiabatic coupling matrix which in turn depends on the time-dependent many-body wavefunctions and excitonic energies[42]. The thermal equilibrium transition rate $\Gamma_{I,J}$ between two excitonic states I and J can be estimated as[56]

$$\Gamma_{I,J} = \begin{cases} \gamma_{I,J}^{\text{Phonon}} \exp\left(-\frac{\omega_J - \omega_I}{k_B T}\right) & if\ \omega_J > \omega_I \\ \gamma_{I,J}^{\text{phonon}} + \gamma_{I,J}^{\text{Dipole}} & if\ \omega_J < \omega_I \end{cases}, \quad (2)$$

where $\gamma_{I,J}^{\text{Phonon}}$ and $\gamma_{I,J}^{\text{Dipole}}$ are transition rates contributed by the phonon-assisted hopping and spontaneous emission, respectively. ω_I and ω_J are exciton energies; k_{B} is the Boltzmann constant and T is temperature. Based on the thermal equilibrium transition rates $\Gamma_{I,J}$, we can perform MC simulations to estimate exciton diffusion length (L_{D}), lifetime (τ), and diffusivity D.

A computational cell comprised of 4 IDIC molecules (560 atoms) is used in the BOMD simulations at three temperatures (100 K, 200 K, 300 K). The IDIC molecules are placed

randomly in the cell, and then relaxed to reach the local equilibrium structure. By varying the dimension of the computational cell, we can obtain its optimized dimension (~18 Å), leading to a mass density of 1.15 g/cm^3 for the IDIC film (Supporting information). The molecules are gradually heated to a desired temperature with velocity rescaling and subsequently kept at the temperature for 2 ps to reach the thermal equilibrium. Finally, a production run based on the microcanonical ensemble is performed for 3 ps at each temperature. The time step in the BOMD simulations is 1 fs and for each time step 8 highest occupied KS orbitals and 12 lowest unoccupied KS orbitals are included in the LR-TDDFT calculations to determine the energies and wavefunctions of these 96 excitons. To confirm that the number of excitons (96) is sufficient, we increase the number of excitons to 192 with 12 highest occupied KS orbitals and 16 lowest unoccupied KS orbitals to calculate the exciton density of states shown in Figure 3. We find that for low energy excitations relevant to exciton diffusion (< 2 eV), the DOS is converged with respect to the number of excitons (96). All first-principles calculations are performed at the Γ point in the Brillouin zone with an energy cutoff of 500 eV, using Projector Augmented-Wave (PAW) pseudopotentials[57] implemented in the VASP package[58]. Grimme's D2 dispersion correction[59] is used to capture the van der Waals interaction between the molecules. Additional information on LR-TDDFT and NAMD calculations can be found in Supporting Information.

To simulate exciton diffusion in a length scale that is relevant to the experiments, the simulation box is multiplied by 31 times in each direction to construct a $31 \times 31 \times 31$ supercell to perform the MC simulations. In each supercell, the exciton wavefunctions are randomly selected from different BOMD snapshots of the home simulation box, and they are then randomly rotated before assigned to each of 100 supercells[42]. In this way, we can model exciton diffusion in a disordered IDIC film comprised of 100 different supercells. However, the IDIC

film modeled in the MC simulations may be more disordered than the IDIC films in the experiments.[8] Hence, the theoretical L_D and D may be slightly lower than the corresponding experimental values. In each supercell, 100 exciton diffusion trajectories are considered, thus in total 10^4 trajectories for each initial exciton state are included in the present work. The exciton diffusion properties are averaged over these 10^4 trajectories.

Results and Discussion

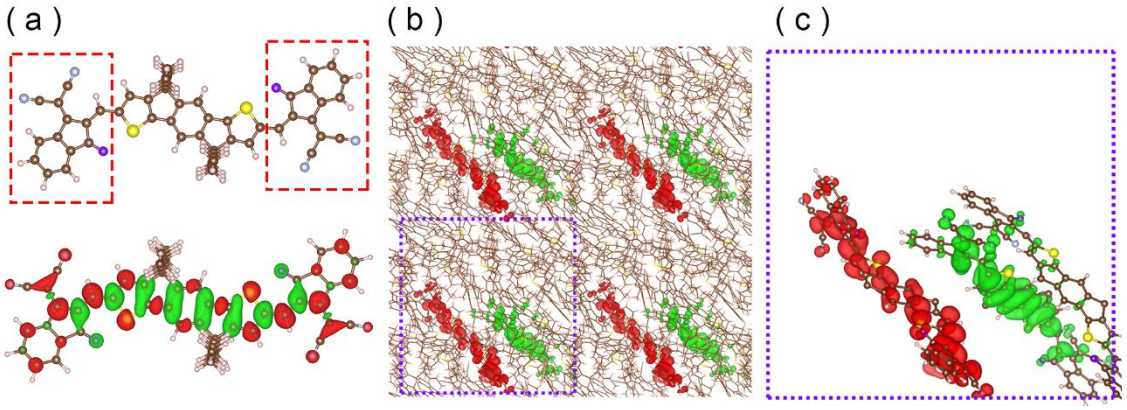

Figure 1. (a) The IDIC molecule (top) and its charge density of the lowest energy exciton (bottom). The brown, gray, white, purple, yellow spheres denote C, N, H, O, and S atoms, respectively. The two terminals of the IDIC molecule are enclosed in dashed boxes. (b) The charge density of the lowest energy exciton in disordered IDIC film. The blown-up view of the purple box is shown in (c). The red (green) iso-surface represents the electron (hole) density at 0.0005e/Å^3.

IDIC has the planar A−D−A molecular structure, shown in Figure 1(a), in which the acceptor group at the two terminals exhibits stronger electron affinity than the donor group at the center. Thus, photo-excited electron is expected to reside at the terminals while the hole at the

center. This expectation is borne out by the charge density distribution of the lowest energy exciton in the IDIC molecule with the formation of a quadrupole moment, as displayed in Figure 1(a). The magnitude of the quadrupole moment is proportional to the intramolecular charge transfer between the donor and acceptor units. Two relevant bandgaps are considered here. The fundamental gap (also called transport or quasiparticle gap) E_g is defined as the difference between the electron affinity and the ionization potential and is calculated as the energy difference between the lowest-unoccupied-molecular-orbital and the highest-occupied-molecular-orbital using the DFT-OTSRSH method. The optical gap E_{opt} is the onset of optical adsorption and is calculated using the TDDFT-OTSRSH method as the energy of the lowest excited state. E_g and E_{opt} of the IDIC molecule are computed as 4.03 eV and 2.45 eV, respectively. The exciton binding energy (E_b) defined as $E_b = E_g - E_{opt}$ is 1.58 eV. These values are close to those obtained by a different first-principles method.[60]

Next, we model a disordered IDIC film by placing 16 IDIC molecules randomly in a simulation box with a dimension of 28.6 Å. We find that the molecular backbones of IDIC are slightly bent during the BOMD simulations but largely maintain their planarity, showing more rigidity than small molecules[61]. After a full relaxation of the molecular structure, we obtained E_{opt} = 1.4 eV for the disordered IDIC film, which is comparable to the experimental value of 1.62 eV.[8] E_g and E_b are 1.9 eV and 0.5 eV, respectively for the disordered film. Compared to the IDIC molecule, these values are much smaller owing to intermolecular interactions and dielectric screening in the IDIC film. Interestingly, the low-energy excitons in the disordered IDIC film are of *intermolecular* nature, with the electrons and holes separated at *neighboring* molecules, shown in the Figure 1(b)-(c) and Figure S3. In fact, six lowest energy excitons examined here all exhibit the similar charge-separated character. Furthermore, we find that the lowest energy exciton

remains charge-separated at different time steps in the BOMD simulations (Figure S4). These results suggest a robust presence of charge-separated excitons in IDIC, which has important consequences on the photovoltaic performance of IDIC-based OPVs.

To elucidate the origin of charge-separated excitons in IDIC, we consider two IDIC molecules arranged in various intermolecular configurations and examine their excitonic properties. In Figure 2, we display eight most stable intermolecular configurations along with the charge density of the lowest energy exciton in each configuration. The total energy of each configuration relative to that of the most stable one in (a) is also indicated. Interestingly, in the three most stable configurations, the electron-withdrawing terminal of one molecule sits closely to the electron-donating center of the other molecule, as shown in Figure 2(a)-(c). Owing to intramolecular charge transfer between its donor and acceptor units, each IDIC molecule carries an electric dipole. Thus, the quadrupole interaction - the electrostatic interaction among four charges (or three linear charges) - arises between two neighboring IDIC molecules. The quadrupole moment is no-zero if the charge distribution is non-spherical. In fact, the quadrupole moment of IDIC molecule is estimated as 478 Debye·Å, larger than that of a conjugated polymer (286 Debye·Å for P3HT) and DPP small molecules (309 Debye·Å). There is an attractive quadrupole interaction between the two IDIC molecules, which breaks the degeneracy of the two molecules and drives the intermolecular charge separation. The degree of charge separation depends on the strength of the quadrupole interaction, which in turn is determined by the intermolecular arrangement. As shown in Figure 2, the lowest energy exciton is charge-separated in the three configurations with the strongest quadrupole attraction and the lowest total energies. In the other configurations, the lowest energy excitons are of *intramolecular* nature. Thus, we predict that IDIC molecules may self-assemble into a configuration where the donor unit of one

molecule is adjacent to the acceptor unit of the other, driven by photo-induced intermolecular charge transfer. To generalize this prediction to condensed phases (e.g., disordered IDIC film), we further examine the excited states of these configurations by increasing the dielectric constant in the TDDFT-OTRSH calculations from $\varepsilon = 1$ (gas phase) to $\varepsilon = 2.0$ and 4.25. $\varepsilon = 4.25$ corresponds to the dielectric constant of a disordered IDIC solid with a mass density of 1.15 g/cm^3, determined from the density functional perturbation theory calculations and $\varepsilon = 2.0$ corresponds to an IDIC film with a lower mass density. The charge densities of the lowest energy excitons for both cases are shown in Figure S5 and S6 with eight different intermolecular configurations. We find that for $\varepsilon = 2.0$, six lowest energy configurations exhibit intermolecular charge-separation and for $\varepsilon = 4.25$, all eight configurations are charge-separated. Therefore, we conclude that in condensed phases of IDIC, low-energy excitons are also charge-separated owing to quadrupole interaction and dielectric screening. The former is induced by intramolecular charge transfer while the latter is driven by efficient π-electron delocalization. Although the photo-excited electron and hole reside at adjacent molecules, the exciton binding energy remains high (~0.5 eV). Thus, these "charge-separated" excitons in the pure acceptor (IDIC) are similar to the so-called charge-transfer excitons at the donor/acceptor interfaces. In the remaining of the paper, we will reserve the term "charge-separated" excitons for those in IDIC to make a distinction from the interfacial charge-transfer excitons. Note that intramolecular excitons with higher energies are also present in the disordered IDIC film. The charge-separated intermolecular excitons in IDIC are expected to promote interfacial charge separation, which may explain why small energy offsets are often sufficient for hole transfer in NFA-based OPVs[13, 62].

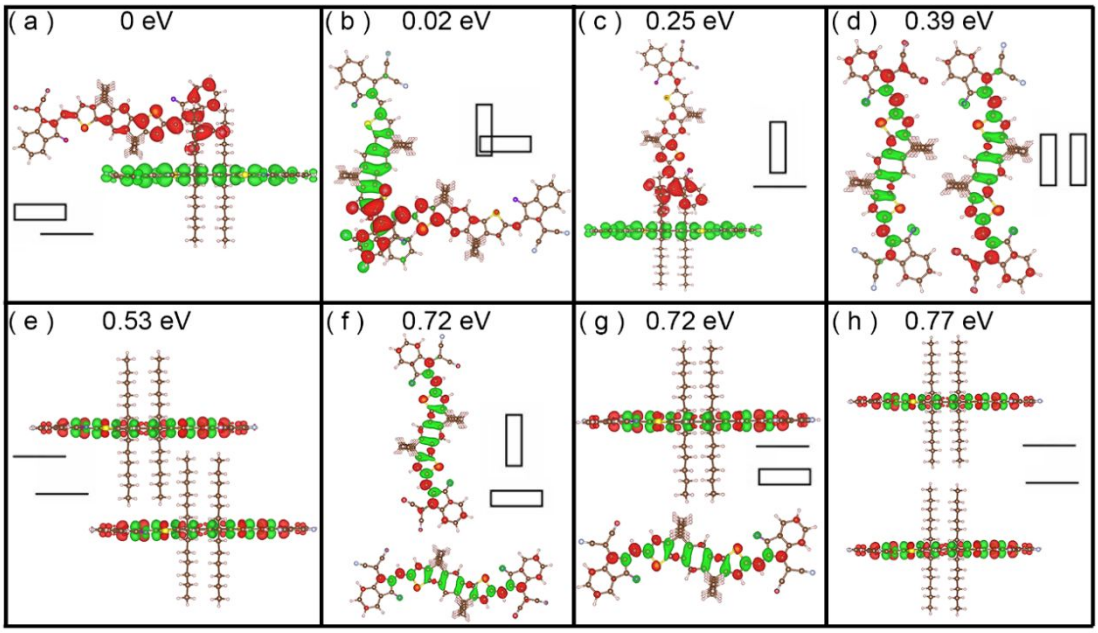

Figure 2. The charge density of the lowest energy exciton in two IDIC molecules arranged in various intermolecular configurations. The total energy of (a) is set to zero. The red (green) iso-surface represents the charge density of electron (hole) at 0.0005 e/Å^3. The rectangle and line in each figure represent the top and side projection of the IDIC backbone, respectively.

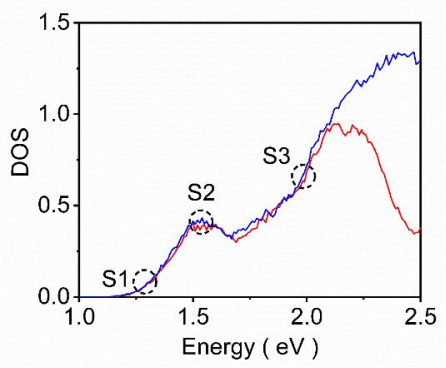

Figure 3. The exciton density of states at 300 K for 96 excitons (red) and 192 excitons (blue). Dashed circles indicate the energy of S1, S2, and S3 excitons.

Exciton diffusion depends on exciton energy, temperature and mass density of the film. In our first-principles studies, we examine three different excitons (S1, S2, and S3) whose initial

energies are indicated in Figure 3. S1 is the lowest energy exciton, and energy of S2 and S3 is 1.5 eV and 2.0 eV, respectively. Three temperatures (100 K, 200 K and 300 K) are considered in our calculations for three different mass densities (1.15, 0.87 and 0.58 g/cm^3) of IDIC film. The exciton density of states is shown in Figure 3 obtained by counting the number of excitonic states at a given energy corresponding to all atomic geometries over the course of the BOMD simulation. The exciton diffusion results from the MC simulations are summarized in Table 1.

At 300 K, we predict that L_D in a disordered IDIC film with a mass density of 1.15 g/cm^3 can reach ~16 nm, corresponding to a domain size of ~32 nm in bulk heterojunctions. This prediction is in line with the large domain sizes of 20-50 nm observed in optimized IDIC blends.[40] L_D could be even larger if the IDIC film is less disordered. We can also estimate exciton harvesting efficiency η defined as:

$$\eta = \int_0^L \frac{p(r)dr}{L},$$

where L is the thickness of the IDIC film and $p(r)$ is the probability that an exciton can be harvested at a distance r from the donor-acceptor interface. Assuming that excitons are generated uniformly in the IDIC film and they will be harvested as long as they reach the interface, we can calculate η as a function of L at 300K. In particular, for S3 exciton (~2.0 eV), the harvesting efficiencies are predicted as 91%, 56%, and 30% for L = 10, 25, 50 nm, respectively. The predicted $\eta = 56\%$ for L = 25 nm matches well the measured external quantum efficiency ~60% in polymer-IDIC bilayer heterojunctions with the same IDIC thickness and photon frequencies ~620 nm (~2 eV).[63] Note, however, the experimental quantum efficiency has contributions from both the donor polymer and IDIC acceptor. The slightly lower η from the MC simulations may be due to the higher degree of disorder in the simulation cell.

Table 1. Exciton diffusion length L_D (nm), lifetime τ (ns), and diffusivity D (10^{-4} cm^2/s) for S1, S2, and S3 excitons in the disordered IDIC film at 100, 200 and 300 K.

	300 K			200 K			100 K		
	S1	S2	S3	S1	S2	S3	S1	S2	S3
L_D	14.7	15.2	16.0	10.3	11.1	12.1	6.8	8.1	9.4
τ	0.95	0.94	0.94	3.6	3.6	3.7	11.2	12.0	12.1
D	31	32.6	35.5	4.0	4.4	4.9	0.6	0.7	0.8

Exciton diffusion is a result of two competing excitonic transitions; the first involves transitions between excited states and the second involves transitions from the excited states to the ground state; both transitions are assisted by thermal fluctuations. At 300 K, the average rate for the first transition (exciton hopping) is 1.3×10^{-3} fs^{-1} and is 1×10^{-6} fs^{-1} for the second transition (exciton decay). As the temperature is lowered from 300 to 100 K, both rates are reduced. As a result, L_D is decreased while τ is increased (Table 1). The decreased L_D combined with increased τ leads to a significant drop in diffusivity D as the temperature is lowered.

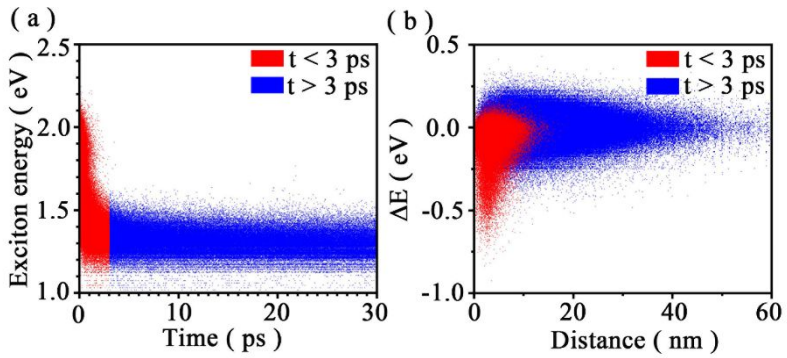

Figure 4. (a) The energy evolution of S3 exciton at 300 K from 10^4 MC trajectories. (b) The exciton energy difference between two adjacent diffusion moves as a function of exciton diffusion distance.

Having examined the temperature dependence, we next study the energy dependence of exciton diffusion. In Figure 4(a), we present the energy of S3 exciton at 300 K as a function of time, with each data point representing the energy of the diffusing exciton at a given time. Two processes can be identified: (1) a downhill diffusion process in which the exciton energy drops from 2.1 eV to 1.5 eV in less than 3 ps (red); (2) a thermally activated process with a minor energy fluctuation between 1.2 and 1.5 eV after 3 ps (blue). The timescale of the first process (~3 ps) is much smaller than the exciton lifetime (~1 ns), and the excess energy (~0.6 eV) of S3 exciton is dissipated into heat, leading to the cooling of the "hot" exciton. The second process involves the dynamics of the thermally equilibrated exciton. In Figure 4(b), we show the energy variation of S3 exciton as a function of its diffusion distance, with a positive (negative) ΔE representing an energy gain (loss). The red color with negative ΔE indicates the cooling process while the blue color with oscillating ΔE corresponds to the thermally activated process. We find that the cooling process has little contribution to exciton diffusion (~5 nm), which is primarily accomplished by the longer and thermally activated process (up to 60 nm). Thus, over-gap

excitations are not expected to yield much increased L_D. While the exciton diffusion processes are not new,[23, 64] the first-principles simulations offer quantitative insights absent in the previous studies.

Table 2. Exciton lifetime τ (ns), diffusivity D (10^{-4} cm^2/s) and diffusion length (L_D) of the lowest energy exciton at 300 K for different materials. The lowest exciton energy $\bar{E}_{S1}$ (eV) averaged during the BOMD simulations, its standard deviation σ (meV) and DOS at S1 are also included. IDIC (75%) and IDIC (50%) represent diluted IDIC film with 75% and 50% mass density of the undiluted IDIC, respectively.

	τ	D	L_D	$\bar{E}_{S1}$	σ	DOS
IDIC	0.95	31	14.7	1.35	74	8.9
IDIC (75%)	3.6	5.8	12.5	1.30	101	4.4
IDIC (50%)	5.5	6.9	16.5	1.26	97	2.8
P3HT	2.3	1.5	5.1	2.67	192	1.5
$DPP(TBFu)_2$	0.5	37.3	11.5	1.67	50	3.8

Next, we address the question whether and how L_D, τ and D may alter quantitatively as a result of charge-separation. To this end, we compare exciton diffusion among IDIC, poly3-hexylthiophene (P3HT) and 3,6-bis(5-(benzofuran-2-yl)thiophen-2-yl)-2,5-bis(2-ethyl-hexyl)pyrrolo[3,4-c]pyrrole-1,4-dione [$DPP(TBFu)_2$]. P3HT is a conjugated polymer whereas $DPP(TBFu)_2$ is a small molecule, and both have been used extensively as donor materials in

OPVs[65, 66]. They are chosen here because they have been studied previously with the similar first-principles framework[42, 67]. The lowest energy excitons in P3HT and DPP(TBFu)$_2$ are of *intramolecular* character with the electron and hole residing at the same molecule or backbone, in contrast to IDIC. Table 2 summarizes the values of L_D, τ and D for the lowest energy excitons in disordered IDIC, P3HT and DPP(TBFu)$_2$ films at 300 K; other relevant quantities are also included for comparison. Since $L_D = \sqrt{D\tau}$, we will focus on D and τ in the following comparison.

We find that D of IDIC is comparable to that of DPP(TBFu)$_2$, but is one order of magnitude greater than that of P3HT. D depends on the excitonic transition rates ($\Gamma_{I,J}$) and the exciton DOS; the greater the transition rates and the DOS, the greater the exciton diffusivity. Both $\Gamma_{I,J}$ and DOS can be computed from the first principles. In particular, as shown in Eqn. (2), $\Gamma_{I,J}$ is proportional to the Boltzmann factor and the phonon-assisted transition rate $\gamma_{I,J}^{\text{Phonon}}$. The Boltzmann factor depends on the energetic disorder (i.e., the thermal fluctuation of exciton energies), which can be estimated as the standard deviation (σ) or the Gaussian width of the exciton energies at different BOMD time steps. The phonon-assisted transition rates, determined by the overlap between the excitonic wavefunctions, are in general of the same order of magnitude among organic semiconductors due to their common π-π stacking. Hence, the difference in $\Gamma_{I,J}$ stems primarily from the energetic disorder. As shown in Table 2, the standard deviation of the lowest energy exciton in IDIC at 300 K is 74 meV, which is comparable to that of DPP(TBFu)$_2$ (50 meV), but much smaller than that of P3HT (192 meV). P3HT has the greatest energetic disorder because it can adopt different conjugation lengths in its backbone and more flexible molecular structures thanks to the rotation of the thiophene ring[68, 69]. In contrast, as small molecules, IDIC and DPP(TBFu)$_2$ have defined structural units and less flexible molecular structures. We have also estimated DOS at S1 whose energy is E_{S1}. As shown in Table 2, IDIC

has a larger DOS than DPP(TBFu)$_2$ and P3HT, indicating that more excitonic states are available for S1 to hop into. Therefore, the higher DOS combined with the lower energetic disorder in IDIC yields greater D over P3HT. As $\Gamma_{I,J}$ depends exponentially on σ, but linearly on DOS, D of IDIC is smaller than that of DPP(TBFu)$_2$.

Exciton lifetime τ is determined by the phonon-assisted nonradiative recombination rate γ_{J0} (which is orders of magnitude higher than the spontaneous recombination rate) by the following expression:

$$\frac{1}{\tau} = \gamma_{J0} \propto \hbar \left\langle \Phi_J \left| \frac{\partial}{\partial t} \right| \Phi_0 \right\rangle = \frac{\langle \Phi_J | \nabla_R H | \Phi_0 \rangle}{E_J} \dot{R} \quad (3)$$

Here, Φ_J and Φ_0 are the wavefunctions of the J-th excitonic state and the ground state, respectively; $\hbar$ is the Planck constant and $\dot{R}$ is the average nuclear velocity. Thus, τ is roughly proportional to the exciton energy E_J, and inversely proportional to the overlap coupling matrix and the nuclear velocity. In terms of the Slater determinants, we have shown that the overlap coupling between the excited and the ground states can be represented by the overlap coupling between the electron and hole wavefunctions of the exciton[42]; and the nuclear velocity can be estimated by the average phonon frequency associated with the excitonic decay. Fourier transforming the time-evolution of the exciton energy, we can estimate the average phonon frequency leading to the exciton decay (Figure S7). It is found that all three materials share similar average phonon frequencies, thus their contrasting lifetimes are primarily caused by differences in the overlap coupling and the exciton energy. Owing to the presence of charge-separated excitons, the electron-hole wavefunction overlap is the smallest in IDIC, so is its overlap coupling. Thus, IDIC has a longer lifetime, doubling that of DPP(TBFu)$_2$. On the other hand, P3HT has the largest exciton energy E_{S1}, resulting in the longest τ among the three materials. Hence, despite the low bandgap, the charge-separated excitons in IDIC enjoy long

lifetimes. The calculated τ in IDIC at 300 K is 0.95 ns, comparable to the experimental values in similar fused-ring electron acceptors with the A-D-A structure, such as ITIC (0.8 ns)[62], TACIC (1.59 ns)[70], BTP-M (1.57 ns)[71] and Y6 (1.8 ns)[71]. Therefore, the combination of low energetic disorder, high exciton DOS, and the presence of charge-separated excitons in IDIC endows its excitons with high diffusivity, long lifetimes, and large diffusion lengths.

Our prediction that charge-separated excitons can be generated in IDIC is consistent with transient absorption spectroscopy measurements in FTAZ:IDIC blends which suggested that exciting the acceptor component could efficiently generate mobile charges.[40] Similarly, there was a recent report[72] on the observation of very slow (100 ps - 1 ns) and yet efficient photoinduced hole transfer in polymer/NFA blend, which led to a hypothesis that charge-transfer excitons might be generated in the A-D-A NFA (4TIC). This hypothesis also agrees with our prediction that charge-separated excitons can be formed in other A-D-A NFAs. In both cases, the photoinduced hole can diffuse across the interface within the lifetime of the exciton (0.95 ns for IDIC), leading to ground-state bleach of the polymers.

Dilution is a common strategy to engineer exciton diffusion in organic materials.[73] To examine the dilution effect in IDIC, we study the diffusion of the lowest energy exciton in disordered IDIC films with lower mass densities (0.87 g/cm^3 and 0.58 g/cm^3), corresponding to 75% and 50% of the undiluted film, respectively. We keep the same number of IDIC molecules in the simulation box, but increase the dimension of the box accordingly, before a full relaxation of the molecular structure. We find that the lowest energy exciton remains charge-separated, but its spatial separation increases as the mass density is lowered (Figure S8). The increased charge separation yields a longer exciton lifetime, and τ increases from 0.95 to 3.6 and 5.5 ns as the mass density decreases from 100% to 75% and 50%, shown in Table 2. This trend is similar to

diluted SubPc whose exciton lifetime increases from 0.5 to 3.0 ns.[73] Thanks to the increased τ, dilation of 50% in IDIC could boost exciton diffusion length by ~12%. However, the dilation lowers exciton diffusivity due to reduced DOS and increased energetic disorder in the diluted films. In other words, L_D does not vary monotonically with the mass density.[73] Nevertheless, tuning the mass density appears to be a useful strategy to boost exciton diffusion in IDIC films.

Conclusion

Based on the first-principles framework, we have studied exciton diffusion in disordered IDIC, which is a promising NFA for OPVs. We predict that the low energy excitons in IDIC are charge-separated with photo-excited electron and hole residing at neighboring molecules. The charge-separated excitons are found to have longer lifetimes thanks to reduced exciton recombination rates. In addition, the disordered IDIC film is shown to have low energetic disorder and high exciton DOS. Combined with the long lifetime, the disordered IDIC is predicted to have a large exciton diffusion length (~16 nm) at 300 K and a quantum efficiency of 56% in bilayer heterojunctions. We have examined the temperature and energy dependence of exciton diffusion in IDIC and by comparisons to P3HT and $DPP(TBFu)_2$, we elucidate how various physical quantities, such as exciton energy, DOS, energetic disorder, and phonon frequency may affect exciton diffusion. Finally, we show that dilation could be a useful means to increase exciton diffusion length in IDIC. This work provides critical insights for exciton properties and their diffusion in NFAs, which may lead to future materials development for highly efficient OPVs.

Conflicts of interest

The authors declare no competing financial interest.

Acknowledgements

The work at California State University Northridge was supported by the U.S. National Science Foundation (DMR1828019) and the U.S. Army Research Office (W911NF1810473). Zi Li acknowledges the support of the National Natural Science Foundation of China (NSCF) under Grant No 11504025.

References

1. C. Yan, S. Barlow, Z. Wang, H. Yan, A. K.-Y. Jen, S. R. Marder and X. Zhan, *Nat. Rev. Mater.*, 2018, **3**, 18003.
2. P. Cheng, G. Li, X. Zhan and Y. Yang, *Nat. Photonics*, 2018, **12**, 131-142.
3. J. Hou, O. Inganäs, R. H. Friend and F. Gao, *Nat. Mater.*, 2018, **17**, 119-128.
4. C. B. Nielsen, S. Holliday, H.-Y. Chen, S. J. Cryer and I. McCulloch, *Acc. Chem. Res.*, 2015, **48**, 2803-2812.
5. Q. Liu, Y. Jiang, K. Jin, J. Qin, J. Xu, W. Li, J. Xiong, J. Liu, Z. Xiao, K. Sun, S. Yang, X. Zhang and L. Ding, *Sci. Bull.*, 2020, **65**, 272-275.
6. L. Meng, Y. Zhang, X. Wan, C. Li, X. Zhang, Y. Wang, X. Ke, Z. Xiao, L. Ding, R. Xia, H.-L. Yip, Y. Cao and Y. Chen, *Science*, 2018, **361**, 1094-1098.
7. Y. Lin, J. Wang, Z. G. Zhang, H. Bai, Y. Li, D. Zhu and X. Zhan, *Adv. Mater.*, 2015, **27**, 1170-1174.
8. Y. Lin, Q. He, F. Zhao, L. Huo, J. Mai, X. Lu, C.-J. Su, T. Li, J. Wang, J. Zhu, Y. Sun, C. Wang and X. Zhan, *J. Am. Chem. Soc.*, 2016, **138**, 2973-2976.
9. W. Wang, C. Yan, T. K. Lau, J. Wang, K. Liu, Y. Fan, X. Lu and X. Zhan, *Adv. Mater.*, 2017, **29**, 1701308.

10. H. Lin, S. Chen, Z. Li, J. Y. L. Lai, G. Yang, T. McAfee, K. Jiang, Y. Li, Y. Liu, H. Hu, J. Zhao, W. Ma, H. Ade and H. Yan, *Adv. Mater.*, 2015, **27**, 7299-7304.

11. G. Zhang, J. Zhao, P. C. Y. Chow, K. Jiang, J. Zhang, Z. Zhu, J. Zhang, F. Huang and H. Yan, *Chem. Rev.*, 2018, **118**, 3447-3507.

12. J. Liu, S. Chen, D. Qian, B. Gautam, G. Yang, J. Zhao, J. Bergqvist, F. Zhang, W. Ma, H. Ade, O. Inganäs, K. Gundogdu, F. Gao and H. Yan, *Nat. Energy*, 2016, **1**, 16089.

13. Y. Zhong, M. Causa', G. J. Moore, P. Krauspe, B. Xiao, F. Günther, J. Kublitski, R. Shivhare, J. Benduhn, E. BarOr, S. Mukherjee, K. M. Yallum, J. Réhault, S. C. B. Mannsfeld, D. Neher, L. J. Richter, D. M. DeLongchamp, F. Ortmann, K. Vandewal, E. Zhou and N. Banerji, *Nat. Commun.*, 2020, **11**, 833.

14. A. C. Mayer, S. R. Scully, B. E. Hardin, M. W. Rowell and M. D. McGehee, *Mater. Today*, 2007, **10**, 28-33.

15. Y. Lin, F. Zhao, Y. Wu, K. Chen, Y. Xia, G. Li, S. K. K. Prasad, J. Zhu, L. Huo, H. Bin, Z.-G. Zhang, X. Guo, M. Zhang, Y. Sun, F. Gao, Z. Wei, W. Ma, C. Wang, J. Hodgkiss, Z. Bo, O. Inganäs, Y. Li and X. Zhan, *Adv. Mater.*, 2017, **29**, 1604155.

16. Z. Li, X. Zhang, Y. Zhang, C. F. Woellner, M. Kuik, J. Liu, T.-Q. Nguyen and G. Lu, *J. Phys. Chem. C*, 2013, **117**, 6730-6740.

17. M. M. Mandoc, L. J. A. Koster and P. W. M. Blom, *Appl. Phys. Lett.*, 2007, **90**, 133504.

18. Z. Li, X. Zhang, G. Lu and T.-Q. Nguyen, *J. Phys. Chem. C*, 2012, **116**, 1205-1210.

19. B. Yu, L. Huang, H. Wang and D. Yan, *Adv. Mater.*, 2010, **22**, 1017-1020.

20. W. Ma, C. Yang, X. Gong, K. Lee and A. J. Heeger, *Adv. Funct. Mater.*, 2005, **15**, 1617-1622.

21. J. Peet, J. Y. Kim, N. E. Coates, W. L. Ma, D. Moses, A. J. Heeger and G. C. Bazan, *Nat. Mater.*, 2007, **6**, 497-500.

22. J. D. A. Lin, O. V. Mikhnenko, J. Chen, Z. Masri, A. Ruseckas, A. Mikhailovsky, R. P. Raab, J. Liu, P. W. M. Blom, M. A. Loi, C. J. García-Cervera, I. D. W. Samuel and T.-Q. Nguyen, *Mater. Horiz.*, 2014, **1**, 280-285.

23. O. V. Mikhnenko, P. W. M. Blom and T.-Q. Nguyen, *Energy Environ. Sci.*, 2015, **8**, 1867-1888.

24. S. M. Menke and R. J. Holmes, *Energy Environ. Sci.*, 2014, **7**, 499-512.

25. J. D. A. Lin, O. V. Mikhnenko, T. S. van der Poll, G. C. Bazan and T. Q. Nguyen, *Adv. Mater.*, 2015, **27**, 2528-2532.

26. S. Chandrabose, K. Chen, A. J. Barker, J. J. Sutton, S. K. K. Prasad, J. Zhu, J. Zhou, K. C. Gordon, Z. Xie, X. Zhan and J. M. Hodgkiss, *J. Am. Chem. Soc.*, 2019, **141**, 6922-6929.

27. S. C. J. Meskers, J. Hübner, M. Oestreich and H. Bässler, *J. Phys. Chem. B*, 2001, **105**, 9139-9149.

28. C. Madigan and V. Bulović, *Phys. Rev. Lett.*, 2006, **96**, 046404.

29. M. E. Köse, P. Graf, N. Kopidakis, S. E. Shaheen, K. Kim and G. Rumbles, *Chemphyschem*, 2009, **10**, 3285-3294.

30. J.-L. Brédas, D. Beljonne, V. Coropceanu and J. Cornil, *Chem. Rev.*, 2004, **104**, 4971-5004.

31. E. Hennebicq, G. Pourtois, G. D. Scholes, L. M. Herz, D. M. Russell, C. Silva, S. Setayesh, A. C. Grimsdale, K. Müllen, J.-L. Brédas and D. Beljonne, *J. Am. Chem. Soc.*, 2005, **127**, 4744-4762.

32. W. A. Luhman and R. J. Holmes, *Adv. Funct. Mater.*, 2011, **21**, 764-771.

33. S. Raisys, K. Kazlauskas, M. Daskeviciene, T. Malinauskas, V. Getautis and S. Jursenas, *J. Mater. Chem. C*, 2014, **2**, 4792-4798.

34. R. Priestley, A. D. Walser and R. Dorsinville, *Opt. Commun.*, 1998, **158**, 93-96.

35. J. E. Kroeze, T. J. Savenije, M. J. Vermeulen and J. M. Warman, *J. Phys. Chem. B*, 2003, **107**, 7696-7705.

36. C. L. Yang, Z. K. Tang, W. K. Ge, J. N. Wang, Z. L. Zhang and X. Y. Jian, *Appl. Phys. Lett.*, 2003, **83**, 1737-1739.

37. C. Sun, F. Pan, H. Bin, J. Zhang, L. Xue, B. Qiu, Z. Wei, Z.-G. Zhang and Y. Li, *Nat. Commun.*, 2018, **9**, 743.

38. X. Li, F. Pan, C. Sun, M. Zhang, Z. Wang, J. Du, J. Wang, M. Xiao, L. Xue, Z.-G. Zhang, C. Zhang, F. Liu and Y. Li, *Nat. Commun.*, 2019, **10**, 519.

39. Q. Fan, Y. Wang, M. Zhang, B. Wu, X. Guo, Y. Jiang, W. Li, B. Guo, C. Ye, W. Su, J. Fang, X. Ou, F. Liu, Z. Wei, T. C. Sum, T. P. Russell and Y. Li, *Adv. Mater.*, 2018, **30**, 1704546.

40. Y. Lin, F. Zhao, S. K. Prasad, J. D. Chen, W. Cai, Q. Zhang, K. Chen, Y. Wu, W. Ma, F. Gao, J.-X. Tang, C. Wang, W. You, J. M. Hodgkiss and X. Zhan, *Adv. Mater.*, 2018, **30**, 1706363.

41. J. D. Chen, Y. Q. Li, J. Zhu, Q. Zhang, R. P. Xu, C. Li, Y. X. Zhang, J. S. Huang, X. Zhan, W. You and J.-X. Tang, *Adv. Mater.*, 2018, **30**, 1706083.

42. X. Zhang, Z. Li and G. Lu, *Phys. Rev. B*, 2011, **84**, 235208.

43. X. Zhang, Z. Li and G. Lu, *Phys. Rev. B*, 2010, **82**, 205210.

44. G. Wu, Z. Li, X. Zhang and G. Lu, *J. Phys. Chem. Lett.*, 2014, **5**, 2649-2656.

45. X. Zhang, Z. Li and G. Lu, *J. Phys. Condens. Matter*, 2012, **24**, 205801.

46. E. K. U. Gross and W. Kohn, *Phys. Rev. Lett.*, 1985, **55**, 2850.

47. M. A. Marques, N. T. Maitra, F. M. Nogueira, E. K. Gross and A. Rubio, *Fundamentals of time-dependent density functional theory*, Springer Science & Business Media, 2012.

48. S. Refaely-Abramson, M. Jain, S. Sharifzadeh, J. B. Neaton and L. Kronik, *Phys. Rev. B*, 2015, **92**, 081204(R).

49. S. Refaely-Abramson, S. Sharifzadeh, M. Jain, R. Baer, J. B. Neaton and L. Kronik, *Phys. Rev. B*, 2013, **88**, 081204(R).

50. S. Refaely-Abramson, S. Sharifzadeh, N. Govind, J. Autschbach, J. B. Neaton, R. Baer and L. Kronik, *Phys. Rev. Lett.*, 2012, **109**, 226405.

51. L.-y. Huang, X. Zhang, M. Zhang and G. Lu, *Phys. Rev. Materials*, 2018, **2**, 054003.

52. L.-y. Huang, X. Zhang, M. Zhang and G. Lu, *J. Phys. Chem. C*, 2017, **121**, 12855-12862.

53. Y. Gao, M. Zhang, X. Zhang and G. Lu, *J. Phys. Chem. Lett.*, 2019, **10**, 3820-3827.

54. J. Liu, X. Zhang and G. Lu, *Nano Lett.*, 2020, **20**, 4631–4637.

55. A. K. Dhara and S. K. Ghosh, *Phys. Rev. A*, 1987, **35**, 442.

56. P. V. Parandekar and J. C. Tully, *J. Chem. Phys.*, 2005, **122**, 094102.

57. P. E. Blöchl, *Phys. Rev. B*, 1994, **50**, 17953.

58. G. Kresse and J. Furthmüller, *Phys. Rev. B*, 1996, **54**, 11169.

59. S. Grimme, *J. Comput. Chem.*, 2006, **27**, 1787-1799.

60. L. Zhu, Y. Yi and Z. Wei, *J. Phys. Chem. C*, 2018, **122**, 22309-22316.

61. G. Long, A. Li, R. Shi, Y.-C. Zhou, X. Yang, Y. Zuo, W.-R. Wu, U. S. Jeng, Y. Wang, X. Wan, P. Shen, H.-L. Zhang, T. Yan and Y. Chen, *Advanced Electronic Materials*, 2015, **1**, 1500217.

62. X. Liu, Y. Yan, A. Honarfar, Y. Yao, K. Zheng and Z. Liang, *Adv. Sci.*, 2019, **6**, 1802103.

63. T. H. Lee, S. Y. Park, W.-W. Park, X. Du, J. H. Son, N. Li, O.-H. Kwon, H. Y. Woo, C. J. Brabec and J. Y. Kim, *ACS Energy Lett.*, 2020, **5**, 1628-1635.

64. O. V. Mikhnenko, F. Cordella, A. B. Sieval, J. C. Hummelen, P. W. M. Blom and M. A. Loi, *J. Phys. Chem. B*, 2008, **112**, 11601-11604.

65. G. Li, V. Shrotriya, J. Huang, Y. Yao, T. Moriarty, K. Emery and Y. Yang, *Nat. Mater.*, 2005, **4**, 864–868.

66. B. Walker, A. B. Tamayo, X. D. Dang, P. Zalar, J. H. Seo, A. Garcia, M. Tantiwiwat and T. Q. Nguyen, *Adv. Funct. Mater.*, 2009, **19**, 3063-3069.

67. Z. Li, X. Zhang and G. Lu, *J. Phys. Condens. Matter*, 2014, **26**, 185006.

68. J. Liu, I. A. Mikhaylov, J. Zou, I. Osaka, A. E. Masunov, R. D. McCullough and L. Zhai, *Polymer*, 2011, **52**, 2302-2309.

69. S. Ko, E. T. Hoke, L. Pandey, S. Hong, R. Mondal, C. Risko, Y. Yi, R. Noriega, M. D. McGehee, J.-L. Brédas, A. Salleo and Z. Bao, *J. Am. Chem. Soc.*, 2012, **134**, 5222-5232.

70. T. Umeyama, K. Igarashi, D. Sasada, Y. Tamai, K. Ishida, T. Koganezawa, S. Ohtani, K. Tanaka, H. Ohkita and H. Imahori, *Chem. Sci.*, 2020, **11**, 3250-3257.

71. L. Zhan, S. Li, T.-K. Lau, Y. Cui, X. Lu, M. Shi, C.-Z. Li, H. Li, J. Hou and H. Chen, *Energy Environ. Sci.*, 2020, **13**, 635-645.

72. Y. Liu, L. Zuo, X. Shi, A. K.-Y. Jen and D. S. Ginger, *ACS Energy Lett.*, 2018, **3**, 2396-2403.

73. S. M. Menke, W. A. Luhman and R. J. Holmes, *Nat. Mater.*, 2013, **12**, 152-157.

TOC

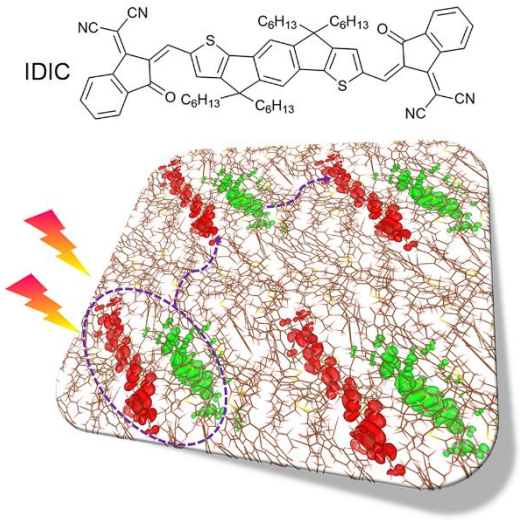
IDIC
NC
CN
S
C_6H_{13}
C_6H_{13}
O
C_6H_{13}
C_6H_{13}
O
S
NC
CN